The Roles of Actin-Binding Domains 1 and 2 in the Calcium-Dependent Regulation of Actin Filament Bundling by Human Plastins

Christopher L. Schwebach[1,2], Richa Agrawal[1], Steffen Lindert[1], Elena Kudryashova[1] and Dmitri S. Kudryashov[1,2]

*1 - **Department of Chemistry and Biochemistry,** The Ohio State University, Columbus, OH 43210, USA*
*2 - **Molecular, Cellular, and Developmental Biology Program,** The Ohio State University, Columbus, OH 43210, USA*

***Correspondence to Dmitri S. Kudryashov:** Department of Chemistry and Biochemistry, The Ohio State University, 484 W 12th Ave, 728 Biosciences Building, Columbus, OH 43210, USA. kudryashov.1@osu.edu*
http://dx.doi.org/10.1016/j.jmb.2017.06.021
Edited by James Sellers

Abstract

The actin cytoskeleton is a complex network controlled by a vast array of intricately regulated actin-binding proteins. Human plastins (PLS1, PLS2, and PLS3) are evolutionary conserved proteins that non-covalently crosslink actin filaments into tight bundles. Through stabilization of such bundles, plastins contribute, in an isoform-specific manner, to the formation of kidney and intestinal microvilli, inner ear stereocilia, immune synapses, endocytic patches, adhesion contacts, and invadosomes of immune and cancer cells. All plastins comprise an N-terminal Ca^{2+}-binding regulatory headpiece domain followed by two actin-binding domains (ABD1 and ABD2). Actin bundling occurs due to simultaneous binding of both ABDs to separate actin filaments. Bundling is negatively regulated by Ca^{2+}, but the mechanism of this inhibition remains unknown. In this study, we found that the bundling abilities of PLS1 and PLS2 were similarly sensitive to Ca^{2+} (pCa_{50} ~6.4), whereas PLS3 was less sensitive (pCa_{50} ~5.9). At the same time, all three isoforms bound to F-actin in a Ca^{2+}-independent manner, suggesting that binding of only one of the ABDs is inhibited by Ca^{2+}. Using limited proteolysis and mass spectrometry, we found that in the presence of Ca^{2+} the EF-hands of human plastins bound to an immediately adjacent sequence homologous to canonical calmodulin-binding peptides. Furthermore, our data from differential centrifugation, Förster resonance energy transfer, native electrophoresis, and chemical crosslinking suggest that Ca^{2+} does not affect ABD1 but inhibits the ability of ABD2 to interact with actin. A structural mechanism of signal transmission from Ca^{2+} to ABD2 through EF-hands remains to be established.

Introduction

The actin cytoskeleton is a complex and ubiquitous eukaryotic system that encompasses hundreds of proteins involved in an array of cellular processes such as cell migration, endocytosis, and cytokinesis [1,2]. Among the over 150 known actin-binding proteins that regulate this intricate system is a subset of actin-bundling proteins responsible for bringing together multiple actin filaments and non-covalently crosslinking them into meshes and bundles [3]. Plastins, also known as fimbrins, are a conserved family of actin-bundling proteins that generate tight bundles of aligned actin filaments in structures such as immune synapses, adhesion contacts, filopodia, and microvilli [4–7].

Plastins are conserved throughout eukaryotic life: yeast and human orthologs share as much as 41% amino acid sequence identity. Functional conservation is also remarkable as two of three human isoforms can rescue the fimbrin deletion phenotype in *Saccharomyces cerevisiae* [8]. In *S. cerevisiae*, fimbrin (Sac6p) is found in actin cables and in endocytic actin patches [9]. Accordingly, loss of Sac6p leads to aberrant cell morphology as well as defects in sporulation and endocytosis [8–10]. Similarly, the *Schizosaccharomyces pombe* fimbrin, Fim1, is involved in endocytosis, cytokinesis, and

polarization [11,12]. A recent work has shown that the only *Caenorhabditis elegans* plastin, PLST-1, is essential for polarization and cytokinesis [13]. The three human plastin isoforms (PLS1, PLS2, and PLS3) share 74%–80% amino acid identity and are expressed in a tissue-specific manner [14]. PLS1, or I-plastin, is primarily expressed in the brush border intestine and kidney epithelia, where it contributes to the structure of the microvilli [15,16]. PLS1 is also expressed in the inner ear epithelium contributing to the stabilization of other cellular protrusions—the hair cell mechanosensing stereocilia [17,18]. PLS2, or L-plastin, is natively expressed in hematopoietic cells and is critical to many immune cell functions including formation of the immune synapse, migration, invasion, and adhesion of hematopoietic cells (neutrophils, lymphocytes, and macrophages) [5,19–24]. A correlation between PLS2 expression by immune cells and their high invasive ability is particularly intriguing, as PLS2 is also ectopically expressed in nearly 70% of epithelial-derived cancers [25], where it contributes to metastatic capabilities of the transformed cells [26–29]. PLS3, or T-plastin, is the most ubiquitous isoform, expressed in all solid tissues [25]. Being the most abundant but least specialized isoform, its cellular role is comparatively less well understood. PLS3 has been shown to contribute to keratinocyte migration through regulation of focal adhesion turnover and it is linked to both endocytosis and DNA repair, but its role in these processes has not been thoroughly investigated [30–33]. Recent work has also shown PLS3 to be important in the development of the epidermal basement membrane in mice [34].

The structure of plastins is unique among actin-bundling proteins. Each plastin consists of an N-terminal regulatory headpiece domain (HP) and two tandem actin-binding domains (ABD1 and ABD2), each consisting of two calponin-homology (CH) domains (Fig. 1) [35]. Simultaneous binding of the ABDs to two separate actin filaments non-covalently crosslinks them into a tight bundle with the centers of nearby filaments separated by ~120 Å [36]. The necessity of both ABDs for bundling has been validated by showing that deletion of ABD2 in human plastin generates a protein that binds but does not bundle actin [37]. Similar results were seen in fission yeast where each ABD is required for efficient crosslinking [11].

High-resolution structures of the actin-binding core (ABD1 and ABD2 only) of plant (*Arabidopsis thaliana*) and yeast (*S. pombe*) fimbrins indicate that the ABDs pack in an antiparallel, cupped, orientation with non-homologous surfaces exposed to the solvent [38]. Cryo-electron microscopy (cryo-EM) reconstruction of ABD2 bound to the filament obtained at 12-Å resolution showed a binding interaction distinct from that of any other tandem CH actin-binding domain [39]. The ABD1–actin interaction could not be reconstructed, however, tentatively due to a multimodal character of binding [39], suggesting that the actin-binding properties of plastins' ABDs are not equivalent.

The N-terminal HP (Fig. 1) is composed of two EF-hand motifs and a ~40-aa-long linker connecting them to ABD1. EF-hands are conserved motifs primarily recognized for their Ca^{2+}-binding capacities [40]. The role of Ca^{2+} binding by the EF-hands is well understood in the context of calmodulin (CaM), which acts as a ubiquitous Ca^{2+} sensor in cells and, upon Ca^{2+} binding, interacts with a CaM-binding motif (CBM) on target proteins regulating their function [41,42]. Plastins contain both EF-hands and a CBM found as a part of the linker immediately following the second EF-hand (Fig. 1) [21,43]. A recent study has shown that there is a Ca^{2+}-dependent intramolecular interaction between these domains, which likely conveys the Ca^{2+} signal from the EF-hands to the actin-binding core [43]. Each of the human plastin isoforms is Ca^{2+}-sensitive and their ability to bundle F-actin is decreased upon Ca^{2+} binding [15,44,45]. Plastins from *Dictyostelium discoideum* and *S. cerevisiae* are also Ca^{2+}-sensitive [46,47]; yet plastins from *Tetrahymena*, *A. thaliana* (Atfim1), and *S. pombe* (Fim1) were reported to bundle F-actin independently of Ca^{2+} [48–50]. The fact that Ca^{2+}-insensitive plastins still retain the N-terminal HP suggests that this region continues to play important structural and/or regulatory roles.

Structures of plant and yeast fimbrin core domains (ABD1 and ABD2 only), human PLS3 ABD1 domain, and the human PLS2 HP were solved by X-ray crystallography or NMR, but the full-length plastin structure has never been solved and how the HP interacts with the core is unknown [38,43,51]. Therefore, it is not understood how a signal from Ca^{2+} binding is conveyed to the ABDs, and binding of which of the ABDs to actin is regulated by Ca^{2+}. These and other questions were addressed in this study, where we compared Ca^{2+} sensitivity of the three human plastin isoforms and confirmed that the bundling, but not binding, ability of each isoform is inhibited by Ca^{2+}. We found that the bundling capacities of PLS1 and PLS2 are similarly sensitive to physiological concentrations of Ca^{2+} (pCa_{50} ~6.4), whereas PLS3 is notably less sensitive (pCa_{50} ~5.9). Finally, using PLS3 and PLS2 plastins and their mutants, we demonstrated that ABD1 is a primary Ca^{2+}-independent F-actin-binding site, while ABD2 is the domain regulated in response to Ca^{2+}.

Results

N-terminal peptide preceding EF-hands domain is dispensable for actin binding and bundling

The canonical EF-hands domain of human plastins is preceded by a short, 7- to 10-aa N-terminal

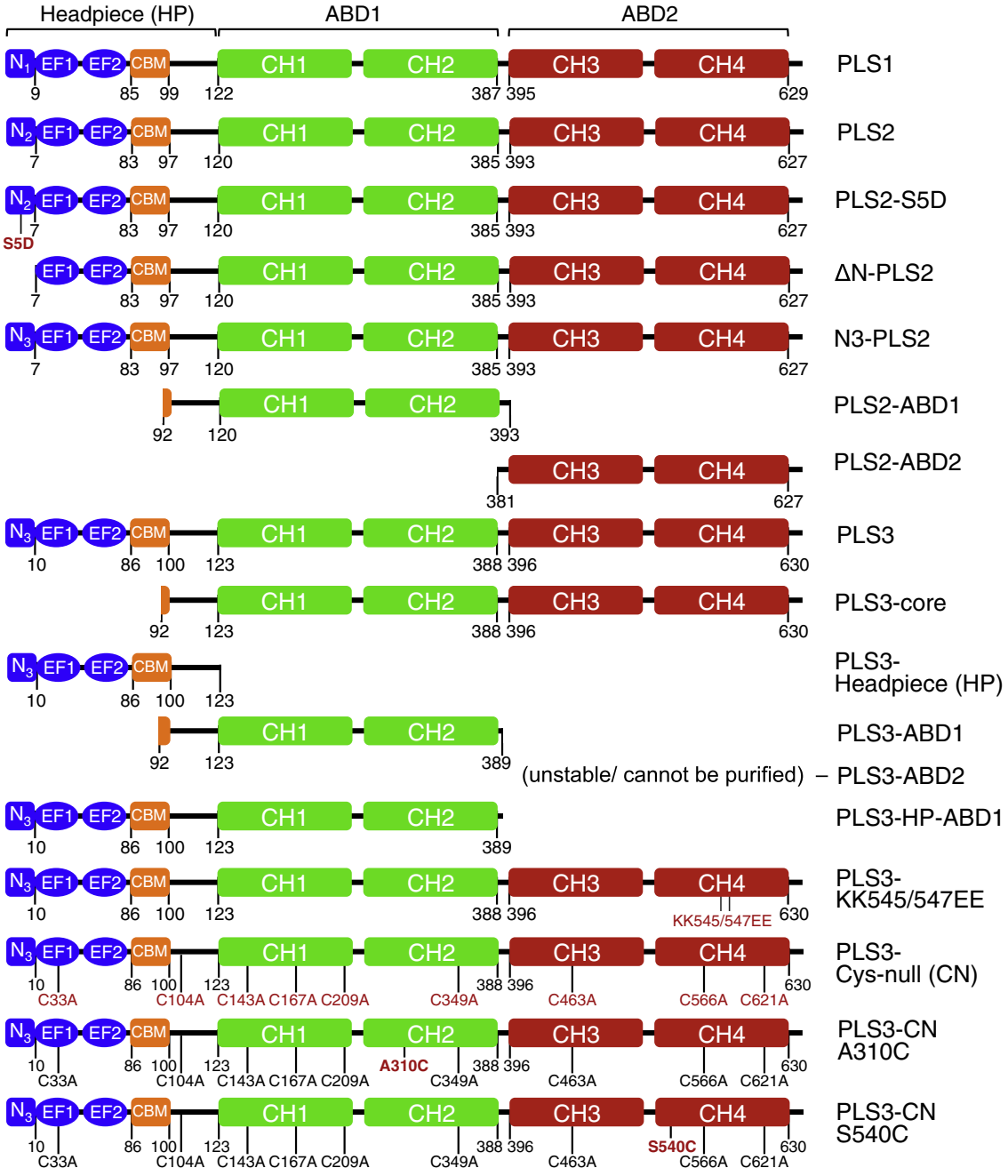

Fig. 1. Domain structure of plastins. Schematic diagrams depict plastin constructs created and used in this study. Numbers represent amino acid residue number in the corresponding protein sequence. Motif and domain designations: $N_{1,2,3}$, N-terminal 7–10-aa sequences of PLS1, PLS2, and PLS3, respectively; EF, EF-hands motifs; CBM, calmodulin-binding motif; Linker, a flexible linker separating the CBM and ABD1; CH, calponin-homology domains; ABD, actin-binding domains; HP, N-terminal regulatory headpiece.

peptide poorly conserved across the isoforms (Fig. 1). A tentative role of the peptide in plastins' function is implied from a reported activation of PLS2 upon phosphorylation of Ser5 both *in vitro* and *in vivo* [7,52–54]. On the other hand, neither PLS3 or PLS1 are known to be phosphorylated nor do they require phosphorylation for their activity. To evaluate the role of the N-terminal peptide in the function of PLS2, we created the following derivatives: a phosphorylation mimic S5D mutant, a construct lacking the

N-terminal 7 aa (ΔN-PLS2), and a mutant with the PLS2 N-terminal peptide replaced by its counterpart from PLS3 (N3-PLS2; Fig. 1). Since all our constructs were expressed with N-terminal 6xHis-tags, the tags were removed by tobacco etch virus protease (TEV protease) with only a single glycine residue left in the remaining constructs. Figure S1 demonstrates that none of the modifications substantially affected the ability of PLS2 to bundle actin *in vitro.* Since the removal of the 6xHis-tags had only relatively minor effect on the activity of the constructs (Fig. S1) but required 3-h-long incubation at room temperature affecting overall protein stability and experimental reproducibility, the 6xHis-tag was not removed in the following experiments.

Human plastins' F-actin bundling activity is inhibited by calcium

To date, the effects of Ca^{2+} on the activity of all three human isoforms of plastins have not been carefully evaluated in a side-by-side comparison. To address this shortcoming, each of the full-length plastin constructs was tested for Ca^{2+} regulation using low-speed (17,000*g*) co-sedimentation to account for the amount of actin bundles formed in the presence of

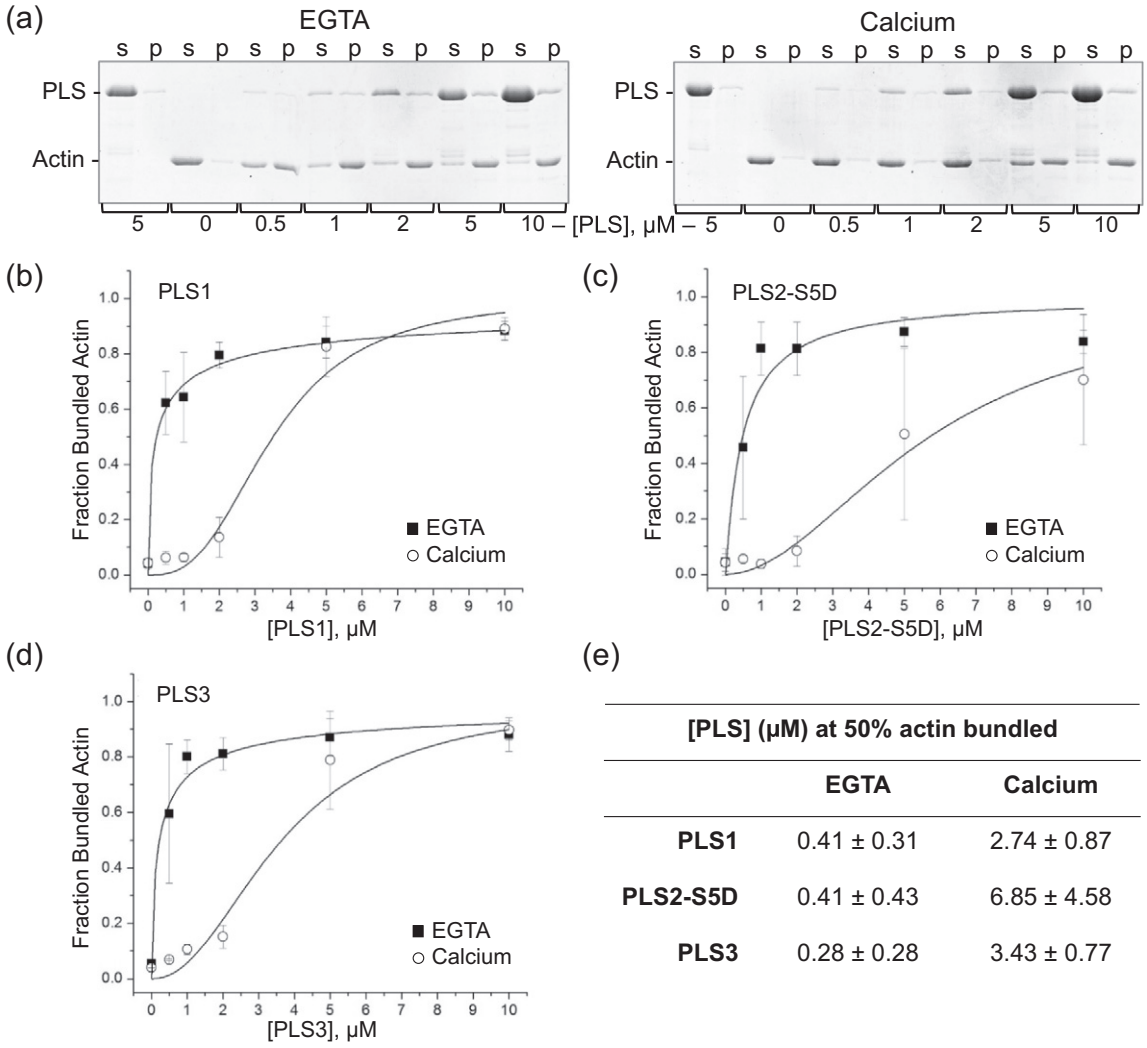

[PLS] (μM) at 50% actin bundled		
	EGTA	**Calcium**
PLS1	0.41 ± 0.31	2.74 ± 0.87
PLS2-S5D	0.41 ± 0.43	6.85 ± 4.58
PLS3	0.28 ± 0.28	3.43 ± 0.77

Fig. 2. Comparison of actin-bundling properties of human plastin isoforms. (a) Representative 9% SDS-PAGE gels of supernatant (s) and pellet (p) fractions after low-speed sedimentation of actin bundles formed by plastin constructs in the absence (EGTA) or presence (calcium) of 0.5 mM free Ca^{2+}. (b–e) Bundling efficiency of PLS1 (b), PLS2-S5D (c), and PLS3 (d) in the presence (open circles) and absence (closed squares) of Ca^{2+} was quantified from gels and expressed as a fraction of bundled actin. Each data point is the average from three independent experiments, with standard deviations represented as error bars. Data were fit to the Hill equation to quantify bundling efficiency expressed as a concentration of plastin at 50% actin bundled (e).

plastin (Fig. 2). Note that under these conditions, only large filament bundles are brought to the pellet, while individual filaments and soluble proteins remain in the supernatant. All plastins were similarly efficient at bundling F-actin when present at sub-stoichiometric ratios in the absence of Ca^{2+}, but this ability was dramatically reduced in the presence of 0.5 mM Ca^{2+} when notable bundling was observed only at 10-fold higher concentrations of plastins (Fig. 2).

Plastin 3 is less sensitive to calcium than plastins 1 and 2

To evaluate the sensitivity of plastin isoforms to Ca^{2+} and elucidate the similarities and differences in the regulation of the isoforms, we monitored the Ca^{2+}-induced disassembly of plastin/F-actin bundles by following a decrease in the intensity of scattered light. Using logistic fitting, we found that both PLS1 and PLS2-S5D showed similar sensitivity to Ca^{2+} (pCa_{50} 6.39 ± 0.03 and 6.34 ± 0.03, respectively), whereas PLS3 was less sensitive (pCa_{50} 5.85 ± 0.03; Fig. 3). Predictably, PLS3-core, a mutant lacking the Ca^{2+}-binding EF-hands (Fig. 1), retained its ability to support actin bundles both at high and low concentrations of Ca^{2+} (Fig. 3).

The EF-hands domain of human plastins binds to the CBM in a calcium-dependent manner

A short sequence highly homologous to conserved CBM has been reported in the linker region between the EF-hands and ABD1 [21,43]. Given that EF-hands of plastins share significant similarity to those of CaM, a Ca^{2+}-dependent interaction between EF-hands and CBM could be expected and was confirmed by a recent report [43]. We independently addressed the effect of Ca^{2+} on susceptibility of the CBM to limited proteolysis. Given that CBM is enriched in basic residues, among several proteases tested, trypsin provided the most convincing data indicating that rapid cleavage at the CBM is strongly inhibited upon the addition of saturating concentrations of Ca^{2+} (Fig. 4a). This protection was observed for all three human plastin isoforms (Fig. S2). The site(s) of the protected cleavage of an N-terminal construct (PLS3-HP) was identified by peptide mass analysis by MALDI-TOF mass spectrometry (Fig. 4b, c). Such prominent protection of the CBM linker region in the presence of Ca^{2+} agrees with a recent finding that EF-hands bind to the linker in a Ca^{2+}-dependent manner [43], and thus elucidates the first in the chain of the events leading to inhibition of the bundling activity of plastins. A bee venom peptide melittin has been recently shown to affect this interaction [43]; however, our data do not confirm this finding in the context of the wild-type PLS3 construct (Fig. S2e), likely due to a higher affinity of the in-cis EF-hands and CBM as compared to that of in-trans EF-hands and melittin.

F-actin binding by all three plastins is unaffected by calcium

Inhibition of bundling may imply that Ca^{2+} weakens F-actin binding to any one or both actin-binding domains of the plastin isoforms. To differentiate

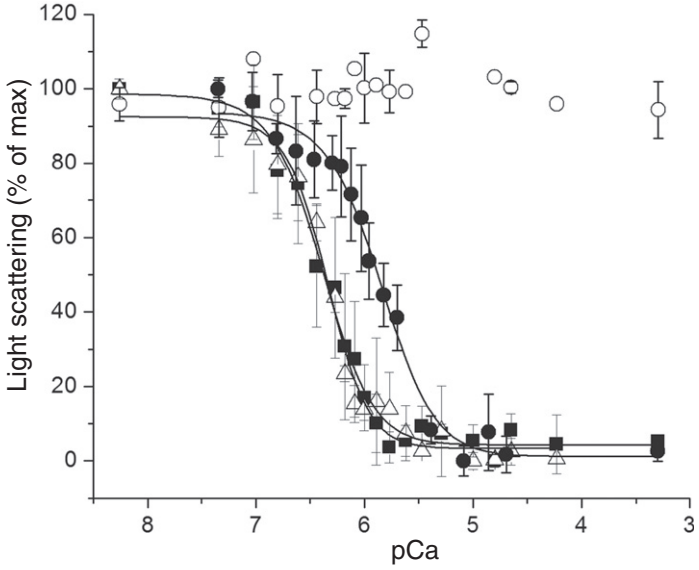

	pCa_{50}
PLS1	6.39 ± 0.03
PLS2-S5D	6.34 ± 0.03
PLS3	5.85 ± 0.03

Fig. 3. Comparison of calcium sensitivities of human plastin isoforms. The dissociation of actin bundles (5 μM) formed in the presence of 1 μM either PLS1 (closed squares), PLS2-S5D (open triangles), PLS3 (closed circles), or the Ca^{2+}-insensitive control, PLS3-core (open circles), upon titration with $CaCl_2$ was monitored via a decrease in light scattering. Each data point is the average from three independent experiments, with standard deviations represented by error bars. Logistic fitting was used to determine calcium sensitivity (pCa_{50}).

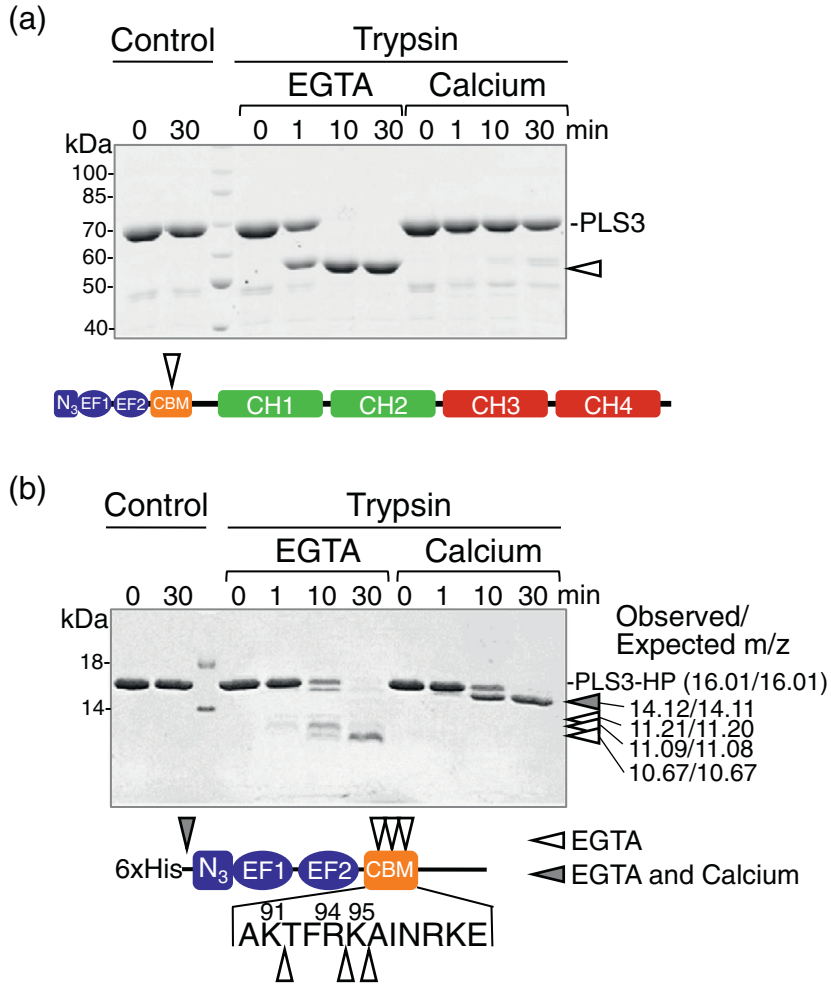

Fig. 4. Protection of the CBM of plastins from proteolysis in the presence of calcium. Limited trypsinolysis of full-length PLS3 (a) and the PLS3 construct truncated immediately prior to ABD1 [HP; (b)] was conducted at 1:250 enzyme to substrate molar ratio in the presence of 2 mM EGTA or 2 mM $CaCl_2$ for indicated time intervals. Arrowheads point to proteolytic products appearing under EGTA-only (white arrowheads) or both EGTA and calcium (gray arrowheads) conditions. Masses of the peptides predicted from sequence (expected) and determined in the experiment by MALDI-TOF (observed) are provided in panel b, while the protected from trypsinolysis residues are indicated on an NMR structure of PLS2 EF-hands–CBM region (PDB: 5J0J; [43]) in panel c. Note that the sequence of PLS3 CBM (90-AKTFRKAIN*R*KE-101) is nearly identical to that of PLS2 (87-AKTFRKAIN*K*KE-99).

between these possibilities, we used high-speed (300,000*g*) co-sedimentation assays, where bound plastin is pelleted together with actin filaments and higher-order structures, while actin monomers and unbound plastins remain in the supernatant. Because plastins have a tendency to aggregate at high

concentrations (above ~30 μM) and thus to pellet independently of actin, we kept plastin concentration low and constant (5 μM) while titrating with increasing concentrations of F-actin (Fig. 5). Although such experimental design does not allow for the assessment of binding stoichiometry, it enables affinity evaluation. Interestingly, all three wild-type plastin isoforms and the PLS2-S5D mutant bound to F-actin with similar affinities, which were virtually unaffected by 1 mM Ca^{2+} (Fig. 5e). This result implies that one of the ABDs of all isoforms of human plastins remains bound to F-actin regardless of the presence of Ca^{2+}, whereas binding of the other ABD is negatively regulated by Ca^{2+}.

Plastin 3 mutant analysis points to ABD2 as the calcium-regulated domain

To determine which ABD domain's binding to actin is inhibited by the EF-hands in response to Ca^{2+}, we

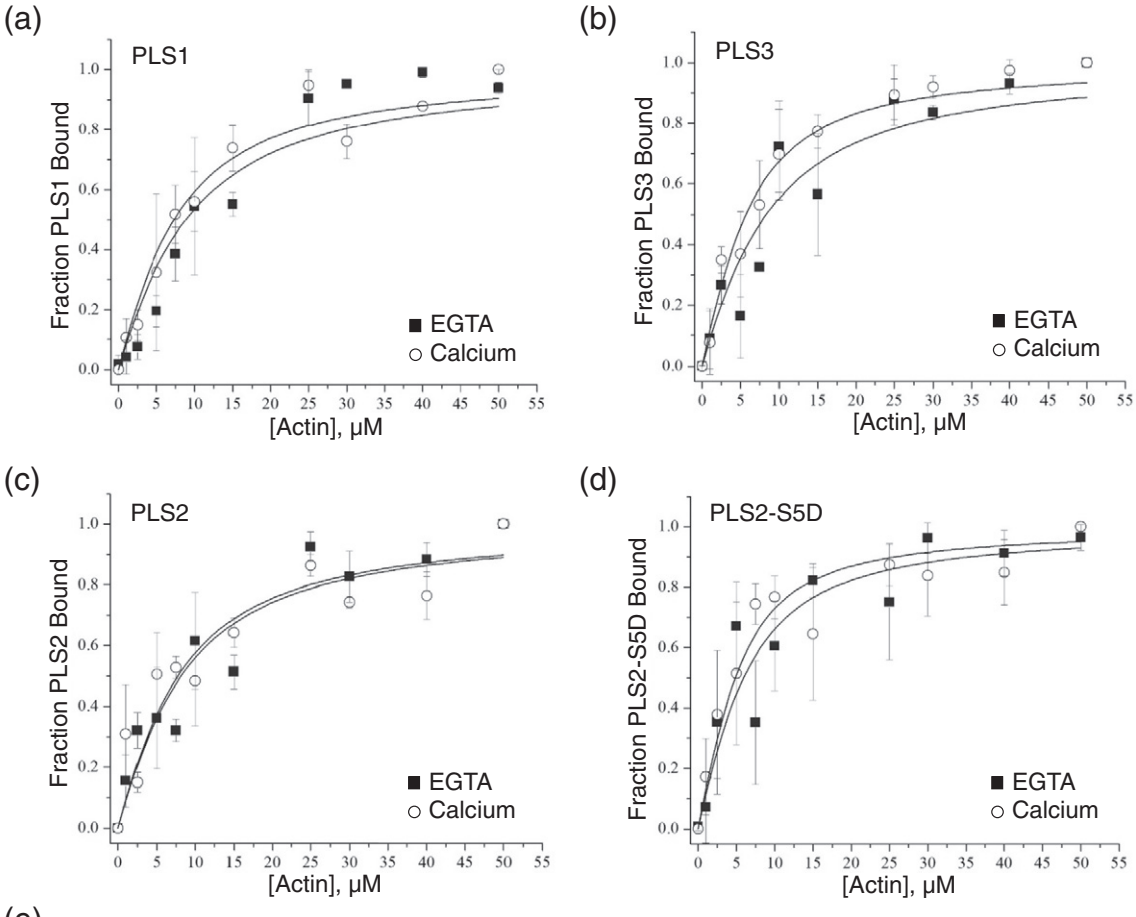

(e)

	K_d (μM)			
	PLS1	**PLS3**	**PLS2**	**PLS2-S5D**
EGTA	5.88 ± 0.74	6.05 ± 1.59	5.66 ± 0.96	3.58 ± 2.56
Calcium	4.91 ± 1.51	3.26 ± 0.19	5.30 ± 1.61	3.83 ± 4.19
p-value	0.523	0.112	0.830	0.909

Fig. 5. Comparison of F-actin binding affinities of human plastins. (a–d) Binding of PLS1 (a), PLS3 (b), PLS2 (c), and PLS2-S5D (d) to F-actin was analyzed by high speed (300,000*g*) co-sedimentation in the absence (closed squares) and presence (open circles) of 1 mM free Ca^{2+}. (e) K_d values were determined by fitting the experimental data to the binding isotherm equation. Each data point is the average from three independent experiments. Error bars represent standard deviations. *p* Values were determined using statistical hypothesis Student's *t* test.

focused on PLS3 and generated two truncation mutants lacking ABD2: a construct containing only ABD1 (ABD1; Fig. 6a) and a construct devoid of ABD2, but containing intact N-terminal HP and ABD1 (HP–ABD1; Fig. 6b). We found that the ABD1 construct bound to F-actin in a Ca^{2+}-independent manner with the affinity similar to that of wild-type PLS3 (Figs. 5e and 6a, g). As for the HP–ABD1 construct, the analysis was complicated due to its molecular weight being similar to that of actin, resulting in overlapping bands on a SDS-polyacrylamide gel and making the quantification impossible. To circumvent this obstacle, we artificially increased the molecular weight of actin at the stage preceding SDS-PAGE analysis by covalently crosslinking it into oligomeric species with an actin-specific toxin ACD produced as one of the domains of MARTX toxin by *Aeromonas hydrophila* (Fig. 6c) [55,56]. Because the crosslinking was conducted after separation of pelleted and unpelleted fractions, it had no influence on the outcome of the experiment. In the presence of Ca^{2+}, about half of the HP–ABD1 population lost the ability to interact with actin (Fig. 6b inset), but the remaining population bound to F-actin with the affinity similar to that of full-length PLS3 (Figs. 5e and 6b, g). Such split in functionality cannot be accounted for by incomplete saturation of Ca^{2+}-binding sites as the concentration of Ca^{2+} exceeded that required for saturation by nearly 0.7 mM. Interestingly, removal of Ca^{2+} via addition of ethylene glycol bis(β-aminoethyl ether) N,N,N′N′-tetraacetic acid (EGTA) to the supernatants of the Ca^{2+}-containing samples restored actin-binding properties of the remaining HP–ABD1 (Fig. 6c). A possible explanation to the observed behavior is a formation of nonfunctional soluble oligomers of HP–ABD1 in the presence of Ca^{2+} due to overall lower stability of the truncated constructs of PLS3. Indeed, $CaCl_2$ decreased the amount of the major HP–ABD1 band observed by native gel electrophoresis from 86.5% to 67.6% by shifting it to the oligomeric species of lower electrophoretic mobility (Fig. 6d). Our attempts to produce isolated PLS3 ABD2 failed as the protein could not be detected upon expression (likely due to a rapid degradation), while an maltose-binding protein (MBP)–ABD2 (a fusion construct with MBP) could be expressed at a low level, but resulted in prompt degradation upon purification, and particularly, upon proteolytic removal of the MBP by TEV protease.

To circumvent the issues of instability caused by the domain separation, we decided to compromise the interaction of ABD2 with F-actin while preserving the overall integrity of the protein. To this end, we employed site-directed mutagenesis to switch charges of two conserved residues in PLS3 ABD2 identical to those found at the binding interface of PLS2 ABD2 with actin [39]. The resulting PLS3 KK545/547EE mutant was unable to bundle F-actin (Fig. 6e), indicating that the goal of weakening ABD2 affinity to actin was achieved. At the same time, the KK545/547EE mutant bound F-actin with K_d similar to that of wild-type PLS3 (Figs. 5e and 6f, g). If ABD1 were the domain whose binding to actin is inhibited by Ca^{2+}, we would expect this mutant to have a reduced affinity in the presence of Ca^{2+}. Instead, we found that binding of the ABD2-inactivated mutant was unaffected by Ca^{2+}, similar to wild-type PLS3 (Figs. 5c and 6f). This, together with their nearly identical affinities for actin (Figs. 5e and 6g), suggests that ABD2 is likely to be the domain whose binding to actin is primarily inhibited by Ca^{2+}-bound EF-hands. Since binding interfaces of ABD1 with F-actin are unknown, our attempts to generate ABD1 mutants with compromised binding to actin were not successful and produced either fully functional proteins (when few mutations were introduced) or nonfunctional proteins with high propensity to precipitation (with multiple charge switch mutations on surface-exposed residues).

The N-terminal HP directly interacts with ABD2 independent of calcium

Next, we tested the hypothesis that the Ca^{2+}-dependent inhibition of ABD2 by EF-hands can be mediated via direct interaction between these domains. Given that the ABD2 construct of PLS3 could not be obtained, we focused on the ABD2 of

Fig. 6. Binding and bundling properties of PLS3 constructs with impaired or deleted ABD2. Binding of PLS3–ABD1 (a) and PLS3-HP–ABD1 (b) truncation mutants was assessed by high-speed co-sedimentation in the absence (closed squares) and presence (open circles) of 1 mM free Ca^{2+}. The addition of Ca^{2+} rendered a population of HP–ABD1 incapable of binding actin. Raw binding data are shown in panel b (inset), whereas the main panel (b) represents normalization of the Ca^{2+} data to the binding saturation point used for the K_d assessment. To prevent the overlap between actin and HP–ABD1 bands on SDS gels, actin was crosslinked to oligomers by ACD toxin added to the pellet fractions upon their separation from supernatants (see Materials and Methods) (c). This effect was reversible as the addition of EGTA restored its ability to bind actin (c). (d) Native gel analysis shows accumulation of low-mobility, high-molecular-weight oligomeric species of HP–ABD1 construct formed in the presence of Ca^{2+}. Bundling (e) and binding (f) abilities of a point mutant of PLS3 KK545/547EE (closed squares and circles) were compared to those of wild-type PLS3 protein (open squares and circles) in the presence of EGTA (squares) or Ca^{2+} (circles). Wild-type PLS3 data are the same as shown in Fig. 2d. (g) K_d values were determined by fitting the data to the binding isotherm equation. Each data point is the average from three independent experiments. Error bars represent standard deviations. *p* Values were determined using statistical hypothesis Student's *t* test.

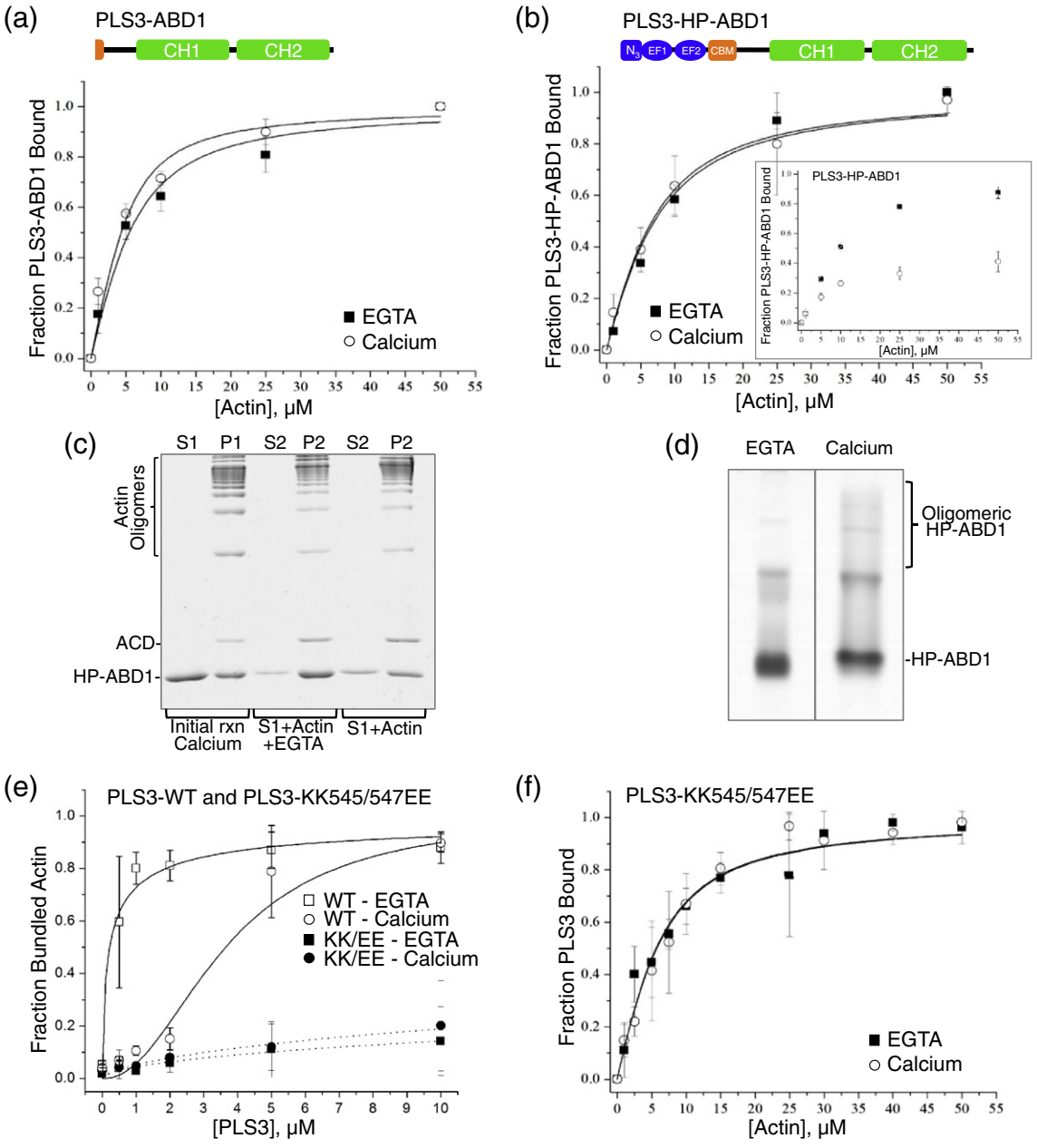

(g)

	K_d (μM)		
	PLS3 ABD1	**PLS3 HP-ABD1**	**PLS3 KK/EE**
EGTA	3.07 ± 1.23	4.54 ± 0.91	2.96 ± 1.07
Calcium	2.05 ± 0.57	4.30 ± 3.02	3.30 ± 1.53
p-value	0.429	0.923	0.838

Fig. 6 (*legend on previous page*)

PLS2, as the two domains share 83% amino acid identity. In three independent experiments, native gel electrophoresis showed the appearance of a complex between the domains (Fig. S3), but the result was not highly reproducible likely owing to a relatively low affinity of the domains. Therefore, to

capture the tentative low-affinity transient interactions, we utilized non-specific covalent crosslinking by glutaraldehyde. Independent of the presence of Ca^{2+}, glutaraldehyde crosslinked the PLS3-HP and PLS2-ABD2 into a new band, which was not present with either protein alone (Fig. 7a). The presence of ABD2 in this band was confirmed by using fluorescein maleimide (FM)-labeled PLS-ABD2 construct (Fig. 7a). Interestingly, PLS3-HP can also be crosslinked to PLS2-ABD1 or PLS3-ABD1 (Fig. 7b, c); however, the resulted band was less intense likely reflecting even lower affinity of the fragments to each other in agreement with no detectable interaction between the fragments in electrophoresis under native conditions (Fig. S3).

Förster resonance energy transfer (FRET) experiments point to ABD1 as the primary, calcium-independent actin-binding site

We utilized FRET to further clarify the role of ABD1 and ABD2 domains in Ca^{2+}-dependent regulation of plastins. If ABD1 were the Ca^{2+}-independent domain, we would expect it to be in close proximity to actin regardless of the presence of Ca^{2+}. To test this, we fluorescently labeled PLS3 at ABD2 or ABD1 at the positions expected to be in close proximity to the actin filament [39]. To this end, a Cys-null (CN) PLS3 construct with all native Cys residues mutated to Ala (PLS3-CN; Fig. 1) has been tested and confirmed to retain its ability to bind and bundle F-actin (Fig. S4). Using this construct as a template, we created several single cysteine mutants by introducing mutations near the known actin-binding site of ABD2 (S540C) and into several surface areas of ABD1 (A221C, A310C, and A356C) with an idea that at least one of them would be in proximity to the actin-binding surface of ABD1 (Fig. 8a). Out of these three, the A310C mutant generated the highest FRET efficiency under conditions of bundling and therefore was used in the following studies. For FRET experiments, actin was labeled at C374 with tetramethylrhodamine maleimide (TMR) to serve as a FRET acceptor and polymerized in the presence of phalloidin to stabilize otherwise unstable TMR–actin filaments [57]. Plastin mutants were labeled with FM as a FRET donor (Fig. 8).

Both fluorescein-labeled A310C and S540C PLS3 mutants retained the ability to bundle TMR-labeled actin (Fig. S4), albeit less efficiently than wild-type PLS3 (Fig. 2d, e) or PLS3-CN (Fig. S4b, c). This reduced bundling ability was possibly a cumulative outcome of the mutations and the presence of the fluorescent probe on plastins and actin and may also reflect aging of plastins due to longer processing time required for labeling. Also, similarly to their background protein PLS3-CN, both mutants demonstrated a reduced sensitivity to Ca^{2+}, likely owing to a desensitizing C33A mutation in the first EF-hand of the Ca^{2+}-binding region (Fig. 1).

If ABD2 were the Ca^{2+}-independent domain, fluorescein at ABD2 S540C would be quenched by 99.0% due to energy transfer given the cryo-EM-derived distance to actin's C374 of 25.7 Å [39] and the Förster distance R_0 of the donor/acceptor pair of 55 Å [58]. However, under all the conditions tested, the

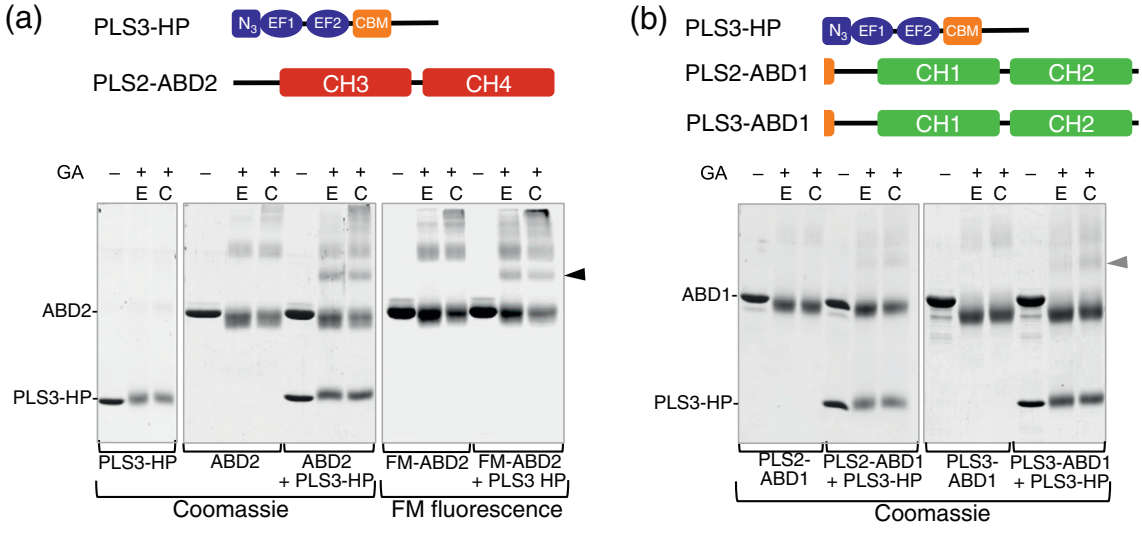

Fig. 7. Interaction of the N-terminal headpiece with actin-binding domains. PLS3-HP construct was mixed with PLS2-ABD2 (a) and PLS2-ABD1 or PLS3-ABD1 (b) in the absence (E = EGTA) or presence (C = calcium) of Ca^{2+} and crosslinked by glutaraldehyde (GA). Crosslinking reactions were resolved on SDS-PAGE. Gels were stained with Coomassie Brilliant Blue, or (in case of FM-labeled PLS2-ABD2) fluorescent images acquired under 365-nm excitation. Arrowheads denote a new band resulting from the GA-crosslinking of PLS3-HP and ABDs.

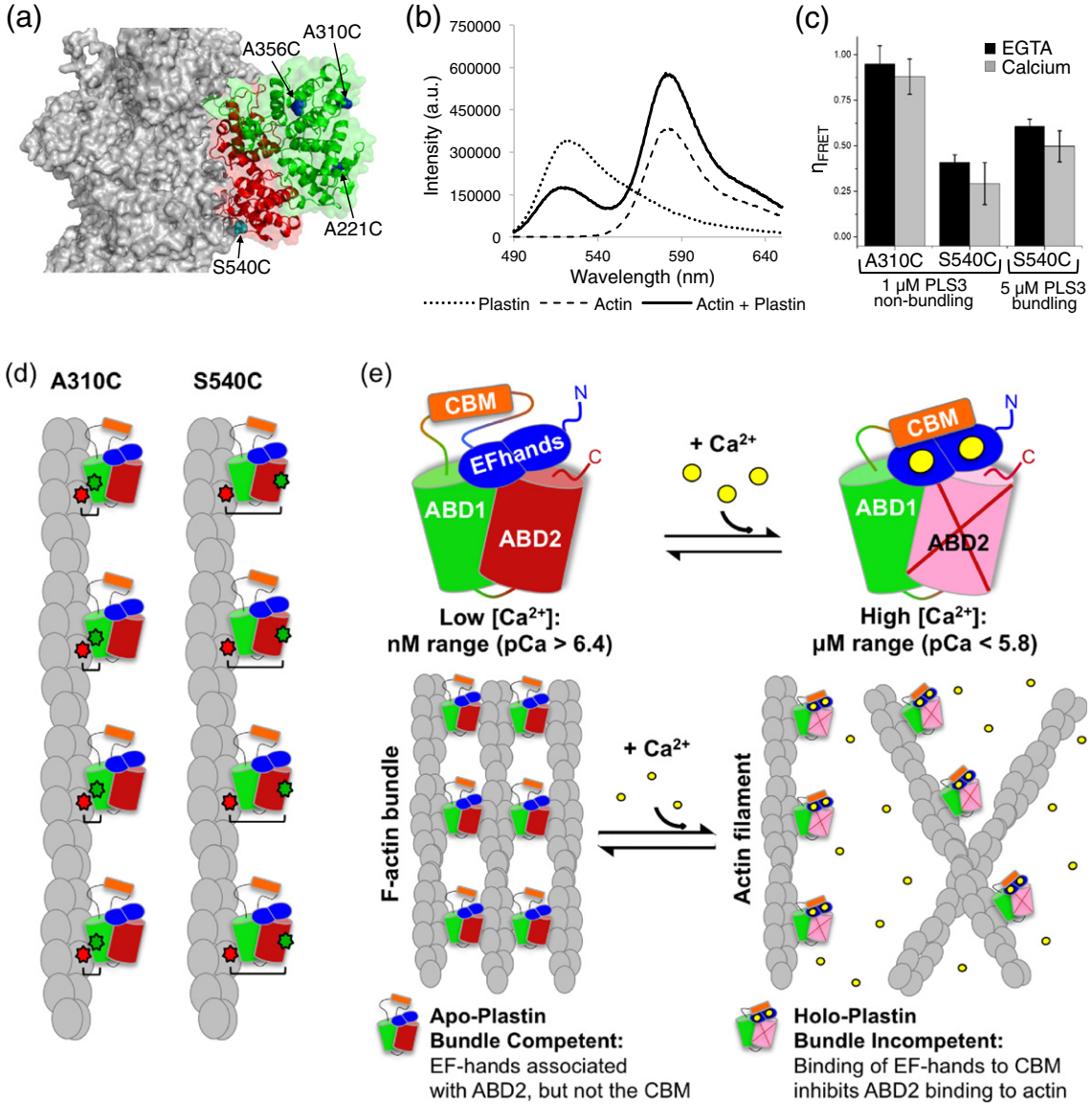

Fig. 8. FRET analysis of ABD1 and ABD2 proximity to actin. (a) Since the actin-binding site on ABD1 (in green) is not known, single cysteines were initially introduced at three different locations (A221C, A310C, A356C; represented as blue spheres) guided based on a homology model of a full-length PLS3 (Phyre.2 [78]) superimposed with the cryo-EM reconstruction (3BYH [33]) of ABD2 (in red) bound to F-actin (in gray). Image was generated using PyMOL (The PyMOL Molecular Graphics System, Version 1.8 Schrödinger, LLC). Cysteine-deficient mutants of PLS3 with a single cysteine residue located either in ABD1 (A310C) or in ABD2 (S540C; represented as a cyan sphere) labeled with FM and F-actin labeled with TMR at C374 were used for FRET studies. (b) FRET efficiency was calculated from a decrease in fluorescence of a donor (i.e., FM moiety on PLS3) in the presence of the acceptor (TMR–actin; solid line) as compared to a donor and unlabeled actin (dotted line). (c) FRET efficiencies between fluorophores at actin's C374 and C310 on ABD1 or C540 on ABD2 were calculated at concentration of fluorescently labeled PLS3 constructs insufficient for bundling (1 μM) and at high (5 μM) "bundling" concentration of PLS3 constructs both in the absence and in the presence of Ca^{2+}. (d) A model suggesting that the ABD1 (in green) of PLS3 is the primary binding site to actin in the presence and absence of Ca^{2+}. Red and green stars represent TMR and FM probes on actin and plastin's ABDs, respectively. (e) Findings of the present study are summarized in the following model: (i) tentatively, the N-terminal headpiece of plastin is associated with its ABD2 domain in the presence and absence of Ca^{2+}; (ii) Ca^{2+} binding by EF-hands leads to their interaction with the CBM; (iii) this interaction is conveyed to a decreased ability of ABD2 to bind actin filaments and, consequently, the diminished ability of the full-length plastin to bundle F-actin; and (iv) the association of the primary plastin's actin-binding domain, ABD1, with actin filament is Ca^{2+}-independent.

probe at the ABD1 A310C was closer to actin as followed from a greater FRET efficiency as compared to that between ABD2 S540C and actin (Fig. 8c, d). This difference was particularly notable under binding/non-bundling conditions (i.e., when only one of the domains is bound to actin) achieved at low ratios of PLS3 to actin (Fig. 8c). These results suggest that ABD1 is the primary, Ca^{2+}-independent domain in close proximity to the filament, when PLS3 is bound but not engaged in bundling.

Under bundling conditions (i.e., at a sufficiently high concentration of PLS3), there was a notable (from 41% to 61%) increase in FRET from ABD2 (Fig. 8c). The increase, however, is not to the degree theoretically predicted for complete binding of ABD2 to the filament under these conditions (99.0%) [39]. Simple calculations suggest that only a small fraction of ABD2 (~20%) contributes to bundling under these conditions. Under both bundling and non-bundling conditions, there was a consistent decrease in FRET between ABD2 and actin upon addition of Ca^{2+}; however, despite its consistency, this difference did not reach statistical significance through triplicate repetitions likely reflecting overall lower sensitivity to Ca^{2+} of all PLS3 mutants with the C33A mutation (Fig. S4).

Discussion

In this study, we carried out a biochemical analysis to establish similarities and differences in the effects of Ca^{2+} on all three human plastin isoforms and addressed the role of individual actin-binding domains in the mechanisms of Ca^{2+}-dependent inhibition of actin bundling. We show that bundling of F-actin by all three isoforms is inhibited upon the addition of Ca^{2+}, and that PLS1 and PLS2 are similarly sensitive to Ca^{2+}, whereas PLS3 is less sensitive. Furthermore, each isoform is able to bind F-actin in a Ca^{2+}-independent manner, implying that binding of only one of the ABDs to F-actin is inhibited. The data obtained by several biochemical and biophysical experimental approaches using point and deletion mutants of PLS3 suggest that ABD2 is the domain whose binding to actin is inhibited by Ca^{2+}, while ABD1 remains bound to actin even in the presence of Ca^{2+}.

The role of Ca^{2+} in regulation of F-actin bundling by human plastins has been recognized for decades [15,44,45], but all three isoforms have never been compared in a single study. Given substantial differences in experimental procedures utilized by various groups, such comparison is essential for establishing isoform-specific functional variations. We found that the bundling, but not binding, activity of all three isoforms is similarly inhibited by Ca^{2+}. This is not entirely predictable given that the N-terminal domains of human plastins are the least similar regions (61% identity between isoforms 1 and 2, and 65% identity between isoforms 1 and 3 and isoforms 2 and 3) as compared to the more conserved actin-binding core (ABD1–ABD2) domains (77%, 78%, and 83% identity between isoforms 1 and 2, 1 and 3, and 2 and 3, respectively). This difference is evolutionary consistent as the core regions of human PLS2 share 42% and 44% identity with those of *S. cerevisiae* and *S. pombe* fimbrins, respectively; whereas the N-terminal domains of these proteins share only 20% and 28% identity.

Despite relatively poor conservation, the N-terminal domains are found in all known plastins/fimbrins, even in the proteins that are known to be insensitive to Ca^{2+} (e.g., *S. pombe* and *A. thaliana* fimbrins) [48,49]. This likely suggests that the N-terminal "headpiece in all plastin orthologs carries conserved function(s) not necessarily correlated with their Ca^{2+}-binding abilities. Regulation is likely to be the primary conserved function, albeit in several cases, the Ca^{2+}-dependent regulation may be replaced by some other regulation mechanisms (e.g., post-translational modifications). Other conserved functions of the N-terminal domain may include structural integration of the ABD domains and/or even actin-binding activities. Both possibilities may account for a recent finding that the PLS2-core (ABD1–ABD2 without the N-terminal HP) fails to promote bundling of actin filaments, while the addition of the CBM and the 23-aa linker connecting it to ABD1 rescues this ability [43]. Whether this effect is due to direct binding of the linker to actin or is mediated via its interaction with the core region is not currently clear. The latter supposition is indirectly supported by our data that the N-terminal headpiece interacts with ABD2 and to a lesser degree with ABD1 and thus may contribute to the stability and function of the full-length protein (Fig. 7).

Several N-terminal amino acids preceding the EF-hands domain have been implicated in functioning of at least PLS2, as phosphorylation of its Ser5 improved PLS2 association with F-actin in cells and potentiated invasiveness of human cancer cells in mice xenograft models, while the S5E substitution promoted F-actin binding and bundling *in vitro* [7]. Surprisingly, we did not observe a notable increase in bundling ability of the PLS2 phosphomimetic mutant S5D (Fig. S1). It is possible that the observed discrepancy stems from an aspartic residue substitution (S5D) in this study *versus* glutamic residues (S5E) used in an older work [7], or some other unaccounted factors. Interestingly, the N-terminal peptides of both PLS1 and PLS3 naturally carry acidic residues at the position 2 (PLS1) or positions 2 and 3 (PLS3), which can tentatively cause effects similar to those achieved by phosphorylation of PLS2 at Ser5. However, substitution of the PLS2

N-terminal peptide with that of PLS3 did not affect the bundling activity of the resulted mutant (Fig. S1). It is conceivable, therefore, that full manifestation of the effects of Ser5 phosphorylation requires additional components (e.g., other protein partners) present in a complex content of the cellular environment.

While this manuscript was in preparation, an NMR study was published demonstrating that Ca^{2+}-induced conformational changes in the EF-hands of PLS2 promote their direct interaction with a predicted CBM located in the linker immediately proximal to EF-hands [43]. Phosphomimetic S5E substitution had no influence on this interaction [43]. Our data fully support this finding by showing that Ca^{2+} causes strong protection of the CBM from proteolysis in all three human plastins (Figs. 4 and S2). However, we did not confirm that a bee venom peptide melittin can affect this interaction in the context of the wild-type PLS3 construct (Fig. S2e), suggesting that the affinity of melittin for EF-hands is insufficient to overcome its interaction with CBM when both regions are present in cis.

Despite this interesting finding, the mechanism of signal transduction from the EF-hands/CBM region to actin-binding domains remains unknown in the absence of a high-resolution structure of a full-length plastin. It has been hypothesized [47] and partially supported by a low-resolution EM-reconstruction study [36] that ABD1 is the domain that becomes occluded in the presence of Ca^{2+}, but the hypothesis has never been challenged biochemically. Therefore, we addressed this question by several independent approaches. Although we indeed observed partial inhibition of the ABD1 interaction with actin (Fig. 6b), it occurred only in the context of a truncated mutant, whose compromised integrity and oligomerization in the presence of Ca^{2+} may have accounted for the observed inhibition (Fig. 6c, d). On the other hand, FRET, bundling, native electrophoresis, and glutaraldehyde crosslinking experiments confidently pointed on ABD2 as the domain, whose binding to actin is primarily inhibited by Ca^{2+}. Particularly, we found that (i) the ABD1 is closer to actin in the presence of Ca^{2+} (Fig. 8c, d), (ii) plastin with a compromised ABD2–actin interface fails to bundle but binds to actin with the affinity indistinguishable of that of isolated ABD1 (Fig. 6e), and (iii) the isolated HP binds to an isolated ABD2 domain (Fig. 7a). Cumulatively, these data strongly suggest that human plastins bind to actin primarily via their ABD1 domain regardless of the presence of Ca^{2+}, while the ABD2 is turned on only upon Ca^{2+} dissociation from the EF-hands (Fig. 8e). Recently, a crosstalk between the regulatory domain and the CH2 subdomain of ABD1 has been proposed to dictate a morphology of the formed bundle by affecting relative orientation of ABD1 and ABD2 domains [59]. Our results neither directly support nor contradict this finding. Our glutaraldehyde crosslinking experiments showing interaction of the headpiece with ABD2 and to a lesser degree ABD1 suggest that the N-terminal headpiece may be positioned close to the ABD1/2 interface and thus be involved in regulation of different aspects of plastin's structure and function.

Our data also indirectly favor a hypothesis that ABD1 is not only the Ca^{2+}-independent, but also the primary site, whose binding to actin precedes binding of ABD2. This hypothesis has been initially proposed by Lebart and coauthors [60] and was largely based on a higher affinity to actin of PLS2 ABD1 (0.34 μM) as compared to ABD2 (2.6 μM) measured by ELISA. We obtained order of magnitude lower affinities for all our plastins to actin, which may be tentatively explained by a use of unmodified proteins and co-sedimentation experiments, which are more reliable than ELISA for quantitative analysis. At the same time, similar affinities for actin between ABD1 and full-length PLS2 observed in the former study are independently confirmed by us for PLS3 (Figs. 5c, e, and 6a, b, f, g), suggesting that this property may be shared by at least human plastins. In this context, the low FRET efficiency between ABD2 and actin filaments is understandable as ABD2 would only be interacting with filaments at crosslinking sites, that is, as rarely as every 13.5 actin subunits (7.4% saturation) in two aligned filaments [36], while ABD1 could be bound at any actin subunit. This is because the proper orientation of two filaments is achieved in a full twist of the helix. A higher density for ABD2 binding under such scenario can be achieved in hexagonal bundles as seen in plastin-mediated bundles in microvilli. However, even under these conditions (three crosslinks every 13.5 actin subunits), there is 22.2% saturation of ABD2 active plastin molecules participating in the bundles, which is in close agreement with the observed ~20% raise in FRET efficiency between ABD2 and actin seen between bundling and binding conditions (Fig. 8c).

The ability of human plastins to bind F-actin in the presence of Ca^{2+} as well as their selectivity toward actin isoforms is a controversial issue [37,44,45,59,61]. Under our experimental conditions, full-length recombinant constructs of all three isoforms of human plastins bound to skeletal α-actin with remarkably similar Ca^{2+}-independent affinities (Fig. 5e). Interestingly, at least for PLS3, the affinity of the full-length protein replicated well that of the ABD1 domain suggesting its leading role in binding (Fig. 6g). It can be envisioned that the ability to stay attached to the filament might be essential for a transient, Ca^{2+}-induced increase in plasticity of actin bundles within microvilli and stereocilia and a prompt recovery of the bundle integrity upon Ca^{2+} removal. Besides, plastins are traditionally considered to be bundling proteins, but some of their activities, particularly those that involve cooperation and competition with other actin-binding proteins, may go beyond Ca^{2+}-dependent regulation of the actin cytoskeleton. Thus, several works in recent years have shown that the interplay between plastins

and other actin-binding proteins is critical for cellular structures and functions. In *S. pombe*, the antagonistic balance between tropomyosin (Cdc8) and cofilin (Adf1) on one hand and plastin (Fim1) and tropomyosin (Cdc8) on another is essential for proper actin dynamics in endocytosis and cytokinesis [62,63]. Also, a balance between several actin-bundling proteins including plastins is critical to maintaining proper cellular structures such as invadopodia, filopodia, and microvilli [64–66]. Some of these events of cooperation and competition may not require bundling (i.e., may persist in the presence of Ca^{2+}), as in one study, the PLS3-HP–ABD1 construct was sufficient to regulate cofilin-mediated actin disassembly in mammalian cell lysate *in vitro* [37].

Our finding that human PLS1 and PLS2 exhibit a 4-fold higher sensitivity to Ca^{2+} (pCa_{50} ~6.4, i.e., ~0.4 μM of Ca^{2+}) than PLS3 (pCa_{50} ~5.9, i.e., ~1.6 μM of Ca^{2+}) may have intriguing implications. It is interesting to compare these data with a previous study on isolated EF-hands motifs, which reported that both sites of PLS2 EF-hands have similar affinity to Ca^{2+} (~1.3 μM), whereas EF-hands of PLS3 have one high and one low-affinity binding sites (~0.4 and 10.6 μM, respectively) [67]. Given that PLS2 with its intermediate Ca^{2+} affinity sites is more responsive to Ca^{2+} than PLS3, which has one site with higher and another with substantially lower affinity, it appears that Ca^{2+} binding to both PLS3 sites is required to manifest the full inhibition. However, it is important to recognize that our experiments did not directly assess the affinity of the plastins' EF-hands for Ca^{2+}. Instead, we measured a more complex phenomenon of bundle dissociation, which is also a function of actin and plastin concentrations, their mutual affinities in the Ca^{2+}-free and Ca^{2+}-bound states, and a critical density of plastin bridges that is sufficient and necessary to hold filaments in the bundles. It is tempting to speculate that a higher sensitivity for Ca^{2+} is one of the key features differentiating PLS1, which is specific for microvilli and stereocilia, from a more ubiquitous PLS3 isoform, which is a major plastin isoform in developing stereocilia, but which is completely replaced by PLS1 upon maturation [68]. Indeed, Ca^{2+} homeostasis plays an important role in dynamic maintenance of microvilli, where PLS1 is a candidate for one of the major Ca^{2+}-responsive and Ca^{2+}-buffering elements tuning the sensitivity of stereocilia to sound waves [69–71]. A properly balanced Ca^{2+}-sensitivity of PLS1 should be essential for both activities. On a similar note, overexpression of the less sensitive PLS3 was linked to an increase in length and width of microvilli in kidney polarized epithelial cells, while expression of the similarly sensitive PLS2 did not [72]. Similarly, a higher Ca^{2+} sensitivity of PLS2, as compared to PLS3, may contribute to its roles in actin-dependent activities of highly motile immune cells and invasive epithelial cancers [19,26–29,65].

To summarize, the data presented here suggest a mechanism by which Ca^{2+} binding to the N-terminal EF-hands domain leads to its interaction with the CBM in the flexible linker connecting the EF-hands and the ABD1 (Fig. 8e). This interaction is conveyed to a decreased ability of ABD2 to bind actin filaments and, consequently, the diminished ability of the full-length plastin to bundle F-actin. The primary plastin's actin-binding domain, ABD1, stays bound to actin filament regardless of Ca^{2+} concentrations. While we have demonstrated that the headpiece directly interacts with ABD2, future studies should address whether ABD2 is inhibited via direct occlusion of its actin-binding site by the EF-hands/CBM region or through an indirect, allosteric mechanism.

Materials and Methods

Protein expression and purification

Actin was prepared from rabbit skeletal muscle acetone powder (Pel-Freeze Biologicals) or chicken skeletal muscle acetone powder [prepared in house from flash-frozen chicken breasts (Trader Joe's)] as previously described [73]. Actin was stored up to 2 weeks on ice in G-buffer [5 mM Tris–HCl (pH 8.0), 0.2 mM $CaCl_2$, 0.2 mM ATP, 5 mM β-mercaptoethanol]. All plastin constructs were cloned as N-terminally 6xHis-tagged proteins into pColdI vector (Clontech) modified to include a TEV protease recognition site downstream the 6xHis-tag. Cloning and site-directed mutagenesis were conducted using the In-Fusion Cloning kit (Clontech). Proteins were expressed in either BL21-Gold(DE3)pLysS *Escherichia coli* or BL21-CodonPlus(DE3)pLysS *E. coli* (Agilent Technologies) grown in nutrient-rich bacterial growth medium [1.25% tryptone, 2.5% yeast extract, 125 mM NaCl, 0.4% glycerol, 50 mM Tris–HCl (pH 8.2)]. After reaching an OD_{600} of 1–1.2, the cells were cooled to 15 °C on ice and expression was induced by the addition of 1 mM IPTG, after which the cells were grown at 15 °C for 15–20 h. All constructs were purified by immobilized metal affinity chromatography on Talon resin (Clontech), eluted in buffer containing 50 mM Hepes (pH 7.4), 300 mM NaCl, 0.1 mM PMSF, 2 mM benzamidine–HCl, and 250 mM imidazole. Proteins requiring further purification were passed over a HiPrep 26/60 Sephacryl S-200 HR size exclusion column (GE Healthcare) using a buffer containing 50 mM Hepes (pH 7.2), 100 mM KCl, 2 mM DTT, and 0.1 mM PMSF. Purified constructs were dialyzed against PLS buffer (10 mM Hepes, 30 mM KCl, 2 mM $MgCl_2$, 0.5 mM EGTA, 2 mM DTT, and 0.1 mM PMSF). Plastin constructs were flash-frozen in liquid nitrogen and stored at −80 °C. Proteolytic removal of the N-terminal 6xHis-tag was accomplished by the addition of 6xHis-tagged

TEV protease at 1:20 mol ratio to plastin constructs followed by 3-h incubation at 25 °C and the removal of the enzyme by immobilized metal affinity chromatography. The removal of the tag had only mild effect on the bundling abilities of all three isoforms (Fig. S1), but was deleterious for protein stability and therefore was not generally applied to the rest of the experiments.

Actin bundling and binding sedimentation assays

Ca^{2+} in the nucleotide cleft of G-actin was switched to Mg^{2+} by adding $MgCl_2$ and EGTA to 0.1 mM and 0.5 mM, respectively, and incubating on ice for 10 min. The Mg^{2+}–G-actin was then polymerized by supplementing $MgCl_2$ to 2 mM, KCl to 30 mM, and Hepes (pH 7.0) to 10 mM, and incubating at room temperature for 30 min. For actin-bundling assays, actin was used at a final concentration of 5 μM; and each plastin, from 0.5 to 10 μM. When required, $CaCl_2$ was added to 0.5 mM free Ca^{2+} concentration (calculated using online resource[†]). For actin-binding reactions, plastins were used at a final concentration of 5 μM; and actin, from 1 to 50 μM. Calcium reactions contained Ca^{2+} at a final free concentration of 1 mM. Reaction mixtures were incubated overnight at 4 °C followed by 1 h at room temperature. Bundling reactions were spun at 25 °C and 17,000*g* for 15 min. Binding reactions were spun at 25 °C and 300,000*g* for 30 min. Supernatants and pellets were carefully separated and analyzed on SDS-polyacrylamide gel, stained with Coomassie Brilliant Blue, and quantified using ImageJ software [74,75]. To quantify bundling efficiency, data were fit to the Hill equation:

$$\%\ \text{Actin Bundled} = \frac{[\text{PLS}]^n}{{K_A}^n + [\text{PLS}]^n},$$

where n is the Hill coefficient and K_A^n is the concentration of plastin at 50% actin bundled.

K_d values were determined by fitting the experimental data to the binding isotherm equation:

$$\text{Fraction PLS Bound} = \frac{P + A + K_d - \sqrt{(P + A + K_d)^2 - 4PA}}{2P},$$

where P is the concentration of plastin and A is the concentration of F-actin.

Light scattering assays

Light scattering for evaluating Ca^{2+} sensitivity of plastins was measured at 90° to the incident light using a FluroMax-3 spectrofluorometer (Jobin Yvon Horiba), with excitation and emission wavelengths set to 330 nm. Polymerized actin (5 μM) was incubated with 1 μM plastin for 1 h at room temperature before measurement. After 1 min of initial measurements, $CaCl_2$ was added at small increments and light scattering was measured for 30 s at 10-s intervals. Buffer composition and calculation of free Ca^{2+} ion concentrations were as described above for actin--bundling experiments. The three measurements for each concentration were averaged and normalized from 0 to 100% bundled actin. The pCa_{50} values were determined by logistic fitting using Origin software (OriginLab).

HP–ABD1/actin-binding sedimentation assays

Binding assays were set up as described above. To circumvent the overlapping actin and HP–ABD1 bands on SDS-gel due to their similar molecular masses, after incubation and sedimentation, pellets were soaked in G-buffer containing gelsolin segment 1 (GS1; 1.2:1 M ratio to total actin) to assist in depolymerization of actin filaments and sequestering G-actin. ACD toxin (purified as described [55]) was added at 1:50 M ratio to actin and incubated at room temperature for 30 min before a second 1:50 addition to ensure complete crosslinking of the actin monomers and therefore shift their mobility above the HP–ABD1 band on the gel (Fig. 6c). To assess binding capabilities of the fraction of HP–ABD1 remaining in the supernatant (S1) after the initial centrifugation with F-actin, S1 was supplemented with either 1 mM EGTA or 1 mM $CaCl_2$ and F-actin was added to a concentration of 25 μM. Reactions were thereafter treated as above including the use of ACD.

Limited trypsinolysis and mass spectrometry

Plastins were diluted to 0.5 mg/mL in cleavage buffer [10 mM Hepes (pH 7.5), 150 mM NaCl] supplemented with either EGTA or $CaCl_2$ (2 mM final concentration). Cleavage was initiated by the addition of trypsin to a final concentration of 2.5 μg/mL, allowed to proceed at 30 °C, and halted at given time points by adding equal volumes of 2× reducing SDS-PAGE sample buffer supplemented with 1 mM PMSF. When indicated, melittin (GenScript) was added to PLS3 at 2:1 M ratio. Mass spectrometry was performed as described [76]. Briefly, peptide masses were confirmed by MALDI-TOF-MS (Bruker Daltonics Microflex) using flexControl 3.3 and flexAnalysis 3.3 software. HCCA was used for the matrix, and Peptide Calibration Standard II (Bruker) was used for calibration. All expected masses are reported as the mass average.

Glutaraldehyde crosslinking assays

Plastin constructs were combined at 10 μM in 20 mM Hepes (pH 7.5) and either 2 mM EGTA or 2 mM $CaCl_2$ and incubated for 1 h at 4 °C. Glutaraldhyde was added to a final concentration of

10 mM, and the reactions were incubated at 37 °C for 5 min. Crosslinking was terminated by the addition of 90 mM Tris–HCl (pH 7.5) before adding equal volume of 2× reducing SDS-PAGE sample buffer.

Native PAGE protein–protein interaction assays

PLS2 ABD1 and ABD2 constructs at 10 μM and PLS3 HP at 20 μM were combined in PLS buffer containing either EGTA or $CaCl_2$ at 2 mM and incubated for 1 h at 4 °C. The reactions were run on non-SDS polyacrylamide gels, cast with the addition of either EGTA or $CaCl_2$, at 4 °C for 2.5 h and otherwise standard conditions except in the absence of SDS.

Labeling proteins with fluorescent probes

To label plastin constructs with FM and actin with TMR, proteins were incubated for 1 h on ice in the presence of 10 mM DTT. Reducing agent was removed by a repeated passing through a NAP5 desalting column (GE Healthcare) equilibrated with G-buffer lacking β-mercaptoethanol. Fluorescent probe was added at 1.5-M excess to protein and incubated overnight on ice. At this point, labeled plastins were passed through a NAP5 column equilibrated with G-buffer to remove excess probe. To enrich TMR-labeled non-polymerizable actin [77], polymerization was initiated as described above and polymerized actin was separated from the labeled actin by centrifugation at 300,000*g* for 30 min at 4 °C. Excess probe was removed from the resulting supernatant by passing it through NAP5 column equilibrated with G-buffer.

FRET experiments

All solutions were degassed prior to the experiment. Actin was polymerized as described above, except that filaments of TMR–actin were stabilized by 1.2-M excess of phalloidin, which does not affect PLS–actin interactions [45]. TMR–actin (FRET acceptor) was added to a final concentration of 5 μM and FM–PLS3 constructs (FRET donors) were added at 1 μM for "non-bundling" and 5 μM for "bundling" conditions, and reactions were incubated at room temperature for 1 h prior to measurement. Unlabeled phalloidin-stabilized actin was used for "donor only" controls to account for potential changes in donor fluorescence upon interaction with actin. Fluorescence emission spectra were measured using FluroMax-3 spectrofluorometer (Jobin Yvon Horiba), with excitation wavelength set to 470 nm. Fluorescence intensities were corrected for the amount of plastin bound to actin as measured by co-sedimentation at high or low speed to assess the extent of binding and bundling as described above. FRET efficiency (η_{FRET}) was calculated by donor quenching and normalized to the bound fraction of plastins using the following equation:

$$\eta_{FRET} = 1 - \frac{I_{DA}}{I_D},$$

where I_{DA} is the intensity of bound donor (FM–PLS) in the presence of acceptor (TMR–actin) and I_D is the intensity of bound donor in the absence of acceptor but presence of unlabeled actin. Fluorescence from free plastin (calculated from pelleting experiments) was assumed to not contribute to FRET and therefore was subtracted from both I_{DA} and I_D values used in the equation. Predicted η_{FRET} for the FM-S540C and TMR–actin pair was calculated by aligning PLS3 (structure modeled using the Phyre2 Web portal [78]) to PLS2 ABD2 bound to F-actin (3BYH; [39]) and measuring the distance between the α-carbons of PLS3 S540 and actin C374. The measured distance was used in the following equation to predict η_{FRET}:

$$\eta_{FRET} = \frac{{R_0}^6}{{R_0}^6 + r^6},$$

where R_0 is the Förster radius of the donor/acceptor pair of (55 Å [58]) and r is the measured distance between PLS3 Ser540 and actin Cys374 (25.7 Å).

Acknowledgments

We would like to thank Mr. Cecil J. Howard for assistance with MALDI-TOF mass spectrometry. This work was supported by an American Cancer Society–sponsored institutional seed grant (GRT00027959; to D.S.K.).

Appendix A. Supplementary data

Supplementary data to this article can be found online at http://dx.doi.org/10.1016/j.jmb.2017.06.021.

Received 19 April 2017;
Received in revised form 30 June 2017;
Accepted 30 June 2017
Available online 8 July 2017

Keywords:
Plastin;
Fimbrin;
EF-hands;
Calcium regulation;
Actin bundling

†http://www.stanford.edu/~cpatton/CaMgATPEGTA-NIST-Plot.htm

Abbreviations used:

PLS1, human plastin 1 or I-plastin; PLS2, human plastin 2 or L-plastin; PLS3, human plastin 3 or T-plastin; ABD, actin-binding domain; CH, calponin-homology domain; HP, headpiece domain; CaM, calmodulin; CBM, calmodulin-binding motif; TEV protease, tobacco etch virus protease; FRET, Förster resonance energy transfer; CN, Cys-null mutant; FM, fluorescein maleimide; TMR, tetramethylrhodamine maleimide; EGTA, ethylene glycol bis(β-aminoethyl ether) N,N,N′N′-tetraacetic acid.

References

[1] T.D. Pollard, J.A. Cooper, Actin, a central player in cell shape and movement, Science 326 (2009) 1208–1212.

[2] T.D. Pollard, G.G. Borisy, Cellular motility driven by assembly and disassembly of actin filaments, Cell 112 (2003) 453–465.

[3] C.A. Schoenenberger, H.G. Mannherz, B.M. Jockusch, Actin: from structural plasticity to functional diversity, Eur. J. Cell Biol. 90 (2011) 797–804.

[4] V. Delanote, J. Vandekerckhove, J. Gettemans, Plastins: versatile modulators of actin organization in (patho)physiological cellular processes, Acta Pharmacol. Sin. 26 (2005) 769–779.

[5] G.H. Wabnitz, T. Kocher, P. Lohneis, C. Stober, M.H. Konstandin, B. Funk, et al., Costimulation induced phosphorylation of L-plastin facilitates surface transport of the T cell activation molecules CD69 and CD25, Eur. J. Immunol. 37 (2007) 649–662.

[6] A. Bretscher, K. Weber, Fimbrin, a new microfilament-associated protein present in microvilli and other cell surface structures, J. Cell Biol. 86 (1980) 335–340.

[7] B. Janji, A. Giganti, V. de Corte, M. Catillon, E. Bruyneel, D. Lentz, et al., Phosphorylation of Ser5 increases the F-actin-binding activity of L-lastin and promotes its targeting to sites of actin assembly in cells, J. Cell Sci. 119 (Pt 9) (2006) 1947–1960.

[8] A.E. Adams, W. Shen, C.S. Lin, J. Leavitt, P. Matsudaira, Isoform-specific complementation of the yeast sac6 null mutation by human fimbrin, Mol. Cell. Biol. 15 (1995) 69–75.

[9] A.E.M. Adams, D. Botstein, D.G. Drubin, Requirement of yeast fimbrin for actin organization and morphogenesis in vivo, Nature 354 (1991) 404–408.

[10] E. Kubler, H. Riezman, Actin and fimbrin are required for the internalization step of endocytosis in yeast, EMBO J. 12 (1993) 2855–2862.

[11] C.T. Skau, D.S. Courson, A.J. Bestul, J.D. Winkelman, R.S. Rock, V. Sirotkin, et al., Actin filament bundling by fimbrin is important for endocytosis, cytokinesis, and polarization in fission yeast, J. Biol. Chem. 286 (2011) 26964–26977.

[12] D. Laporte, N. Ojkic, D. Vavylonis, J.Q. Wu, Alpha-actinin and fimbrin cooperate with myosin II to organize actomyosin bundles during contractile-ring assembly, Mol. Biol. Cell 23 (2012) 3094–3110.

[13] W.Y. Ding, H.T. Ong, Y. Hara, J. Wongsantichon, Y. Toyama, R.C. Robinson, et al., Plastin increases cortical connectivity to facilitate robust polarization and timely cytokinesis, J. Cell Biol. 216 (5) (2017) 1371–1386.

[14] H. Shinomiya, Plastin family of actin-bundling proteins: its functions in leukocytes, neurons, intestines, and cancer, Int. J. Cell Biol. 2012 (2012) 213492.

[15] C.S. Lin, W. Shen, Z.P. Chen, Y.H. Tu, P. Matsudaira, Identification of I-plastin, a human fimbrin isoform expressed in intestine and kidney, Mol. Cell. Biol. 14 (1994) 2457–2467.

[16] E.M. Grimm-Gunter, C. Revenu, S. Ramos, I. Hurbain, N. Smyth, E. Ferrary, et al., Plastin 1 binds to keratin and is required for terminal web assembly in the intestinal epithelium, Mol. Biol. Cell 20 (2009) 2549–2562.

[17] A. Sobin, A. Flock, Immunohistochemical identification and localization of actin and fimbrin in vestibular hair cells in the normal guinea pig and in a strain of the waltzing guinea pig, Acta Otolaryngol. 96 (1983) 407–412.

[18] D. Drenckhahan, K. Engel, D. Hofer, C. Merte, L. Tilney, M. Tilney, Three different actin filament assemblies occur in every hair cell: each contains a specific actin crosslinking protein, J. Cell Biol. 112 (1991) 641–651.

[19] S.C. Morley, The actin-bundling protein L-plastin: a critical regulator of immune cell function, Int. J. Cell Biol. 2012 (2012) 935173.

[20] S.L. Jones, J. Wang, C.W. Turck, E.J. Brown, A role for the actin-bundling protein L-plastin in the regulation of leukocyte integrin function, Proc. Natl. Acad. Sci. U. S. A. 95 (1998) 9331–9336.

[21] G.H. Wabnitz, P. Lohneis, H. Kirchgessner, B. Jahraus, S. Gottwald, M. Konstandin, et al., Sustained LFA-1 cluster formation in the immune synapse requires the combined activities of L-plastin and calmodulin, Eur. J. Immunol. 40 (2010) 2437–2449.

[22] T. Ma, K. Sadashivaiah, N. Madayiputhiya, M.A. Chellaiah, Regulation of sealing ring formation by L-plastin and cortactin in osteoclasts, J. Biol. Chem. 285 (2010) 29911–29924.

[23] S.C. Morley, C. Wang, W.L. Lo, C.W. Lio, B.H. Zinselmeyer, M.J. Miller, et al., The actin-bundling protein L-plastin dissociates CCR7 proximal signaling from CCR7-induced motility, J. Immunol. 184 (2010) 3628–3638.

[24] E.M. Todd, L.E. Deady, S.C. Morley, The actin-bundling protein L-plastin is essential for marginal zone B cell development, J. Immunol. 187 (2011) 3015–3025.

[25] C.S. Lin, T. Park, Z.P. Chen, J. Leavitt, Human plastin genes: comparative gene structure, chromosome location, and differenctial expression in normal and neoplastic cells, J. Biol. Chem. 268 (1993) 2781–2792.

[26] S.M. Riplinger, G.H. Wabnitz, H. Kirchgessner, B. Jahraus, F. Lasitschka, B. Schulte, et al., Metastasis of prostate cancer and melanoma cells in a preclinical in vivo mouse model is enhanced by L-plastin expression and phosphorylation, Mol. Cancer 13 (2014) 10, http://dx.doi.org/10.1186/1476-4598-13-10.

[27] S. Chaijan, S. Roytrakul, A. Mutirangura, K. Leelawat, Matrigel induces L-plastin expression and promotes L-plastin-dependent invasion in human cholangiocarcinoma cells, Oncol. Lett. 8 (2014) 993–1000.

[28] M. Klemke, M.T. Rafael, G.H. Wabnitz, T. Weschenfelder, M.H. Konstandin, N. Garbi, et al., Phosphorylation of ectopically expressed L-plastin enhances invasiveness of human melanoma cells, Int. J. Cancer 120 (2007) 2590–2599.

[29] E. Foran, P. McWilliam, D. Kelleher, D.T. Croke, A. Long, The leukocyte protein L-plastin induces proliferation, invasion and loss of E-cadherin expression in colon cancer cells, Int. J. Cancer 118 (2006) 2098–2104.

[30] H. Ikeda, Y. Sasaki, T. Kobayashi, H. Suzuki, H. Mita, M. Toyota, et al., The role of T-fimbrin in the response to DNA damage: silencing of T-fimbrin by small interfering RNA sensitizes human

liver cancer cells to DNA-damaging agents, Int. J. Oncol. 27 (2005) 933–940.
[31] M. Hagiwara, H. Shinomiya, M. Kashihara, K. Kobayashi, T. Tadokoro, Y. Yamamoto, Interaction of activated Rab5 with actin-bundling proteins, L- and T-plastin and its relevance to endocytic functions in mammalian cells, Biochem. Biophys. Res. Commun. 407 (2011) 615–619.
[32] C. Brun, A. Demeaux, F. Guaddachi, F. Jean-Louis, T. Oddos, M. Bagot, et al., T-plastin expression downstream to the calcineurin/NFAT pathway is involved in keratinocyte migration, PLoS One 9 (2014), e104700.
[33] M. Wottawa, S. Naas, J. Bottger, G.J. van Belle, W. Mobius, N.H. Revelo, et al., Hypoxia-stimulated membrane trafficking requires T-plastin, Acta Physiol (Oxford) (2017), http://dx.doi.org/10.1111/apha.12859.
[34] E. Dor-On, S. Raviv, Y. Cohen, O. Adir, K. Padmanabhan, C. Luxenburg, T-plastin is essential for basement membrane assembly and epidermal morphogenesis, Sci. Signal. 10 (481) (2017) (pii: eaal3154).
[35] M.V. de Arruda, S. Watson, C.S. Lin, J. Leavitt, P. Matsudaira, Fimbrin is a homologue of the cytoplasmic phosphoprotein plastin and has domains homologous with calmodulin and actin gelation proteins, J. Cell Biol. 111 (1990) 1069–1079.
[36] N. Volkmann, D. DeRosier, P. Matsudaira, D. Hanein, An atomic model of actin filaments cross-linked by fimbrin and its implications for bundle assembly and function, J. Cell Biol. 153 (2001) 947–956.
[37] A. Giganti, J. Plastino, B. Janji, M. Van Troys, D. Lentz, C. Ampe, et al., Actin-filament cross-linking protein T-plastin increases Arp2/3-mediated actin-based movement, J. Cell Sci. 118 (2005) 1255–1265.
[38] M.G. Klein, W. Shi, U. Ramagopal, Y. Tseng, D. Wirtz, D.R. Kovar, et al., Structure of the actin crosslinking core of fimbrin, Structure 12 (2004) 999–1013.
[39] V.E. Galkin, A. Orlova, O. Cherepanova, M.C. Lebart, E.H. Egelman, High-resolution cryo-EM structure of the F-actin-fimbrin/plastin ABD2 complex, Proc. Natl. Acad. Sci. U. S. A. 105 (2008) 1494–1498.
[40] A. Lewit-Bentley, S. Rety, EF-hand calcium-binding proteins, Curr. Opin. Struct. Biol. 10 (2000) 637–643.
[41] A. Villarroel, M. Taglialatela, G. Bernardo-Seisdedos, A. Alaimo, J. Agirre, A. Alberdi, et al., The ever changing moods of calmodulin: how structural plasticity entails transductional adaptability, J. Mol. Biol. 426 (2014) 2717–2735.
[42] K. Mruk, B.M. Farley, A.W. Ritacco, W.R. Kobertz, Calmodulation meta-analysis: predicting calmodulin binding via canonical motif clustering, J. Gen. Physiol. 144 (2014) 105–114.
[43] H. Ishida, K.V. Jensen, A.G. Woodman, M.E. Hyndman, H.J. Vogel, The calcium-dependent switch helix of L-plastin regulates actin bundling, Sci Rep 7 (2017) 40662.
[44] Y. Namba, M. Ito, Y. Zu, K. Shigesada, K. Maruyama, Human T cell L-plastin bundles actin filaments in a calcium dependent manner, J. Biochem. 112 (1992) 503–507.
[45] A.N. Lyon, R.H. Pineda, T. Hao le, E. Kudryashova, D.S. Kudryashov, C.E. Beattie, Calcium binding is essential for plastin 3 function in Smn-deficient motoneurons, Hum. Mol. Genet. 23 (2014) 1990–2004.
[46] J. Prassler, S. Stocker, G. Marriott, M. Heidecker, J. Kellermann, G. Gerisch, Interaction of a dictyostelium member of the plastin/fimbrin family with actin filaments and actin–myosin complexes, Mol. Biol. Cell 8 (1997) 83–95.
[47] D. Cheng, J. Marner, P.A. Rubenstein, Interaction in vivo and in vitro between the yeast fimbrin, SAC6P, and a polymerization-defective yeast actin (V266G and L267G), J. Biol. Chem. 274 (1999) 35873–35880.
[48] K. Nakano, K. Sotoh, A. Morimatsu, M. Ohnuma, I. Mabuchi, Interaction among a fimbrin, a capping protein, and an actin-depolymerizing factor in organization of the fission yeast actin cytoskeleton, Mol. Biol. Cell 12 (2001) 3515–3526.
[49] D.R. Kovar, C.J. Staiger, E.A. Weaver, D.W. McCurdy, AtFim1 is an actin filament crosslinking protein from *Arabidopsis thaliana*, Plant J. 24 (2000) 625–636.
[50] S. Shirayama, Tetrahymena fimbrin localized in the division furrow bundles actin filaments in a calcium-independent manner, J. Biochem. 134 (2003) 591–598.
[51] S.C. Goldsmith, N. Pokala, W. Shen, A.A. Fedorov, P. Matsudaira, S.C. Almo, The structure of an actin-crosslinking domain from human fimbrin, Nat. Struct. Biol. 4 (1997) 708–712.
[52] C.S. Lin, A. Lau, T.F. Lue, Analysis and mapping of plastin phosphorylation, DNA Cell Biol. 17 (1998) 1041–1046.
[53] H. Shinomiya, A. Hagi, M. Fukuzumi, M. Mizobuchi, H. Hirata, S. Utsumi, Complete primary structure and phosphorylation site of the 65-kDa macrophage protein phosphorylated by stimulation with pacterial lipoplysaccharide, J. Immunol. 154 (1995) 3471–3478.
[54] S.W. Henning, S.C. Meuer, Y. Samstag, Serine phosphorylation of a 67-kDa protein in human T lymphocytes represents an accessory receptor-mediated signaling event, J. Immunol. 152 (1994) 4808–4815.
[55] E. Kudryashova, D. Heisler, A. Zywiec, D.S. Kudryashov, Thermodynamic properties of the effector domains of MARTX toxins suggest their unfolding for translocation across the host membrane, Mol. Microbiol. 92 (2014) 1056–1071.
[56] D. Heisler, E. Kudryashova, D.O. Grinevich, C. Suarez, J.D. Winkelman, K.G. Birukov, et al., ACD toxin-produced actin oligomers poison formin-controlled actin polymerization, Science 349 (2015) 535–539.
[57] D.S. Kudryashov, M. Phillips, E. Reisler, Formation and destabilization of actin filaments with tetramethylrhodamine-modified actin, Biophys. J. 87 (2004) 1136–1145.
[58] A.G. Byrne, M.M. Byrne, G. Coker Iii, K.B. Gemmill, C. Spillmann, I. Medintz, et al., Data, FRET—Förster Resonance Energy Transfer, Wiley-VCH Verlag GmbH & Co. KGaA 2013, pp. 655–755.
[59] R. Zhang, M. Chang, M. Zhang, Y. Wu, X. Qu, S. Huang, The structurally plastic CH2 domain is linked to distinct functions of fimbrins/plastins, J. Biol. Chem. 291 (2016) 17881–17896.
[60] M.C. Lebart, F. Hubert, C. Boiteau, S. Venteo, C. Roustan, Y. Benyamin, Biochemical characterization of the L-plastin–actin interaction shows a resemblance with that of A-actinin and allows a distinction to be made between the two actin-binding domains of the molecule, Biochemistry 43 (2004) 2428–2437.
[61] M. Pacaud, J. Derancourt, Purification and further characterization of macrophage 70-kDa protein, a calcium-regulated, actin-binding protein identical to L-plastin, Biochemistry 32 (1993) 3448–3455.
[62] C.T. Skau, D.R. Kovar, Fimbrin and tropomyosin competition regulates endocytosis and cytokinesis kinetics in fission yeast, Curr. Biol. 20 (2010) 1415–1422.
[63] J.R. Christensen, G.M. Hocky, K.E. Homa, A.N. Morganthaler, S.E. Hitchcock-DeGregori, G.A. Voth, et al., Competition between tropomyosin, fimbrin, and ADF/cofilin drives their sorting to distinct actin filament networks, eLIFE 6 (2017) 1–31 (pii: e23152).

[64] J.D. Winkelman, C. Suarez, G.M. Hocky, A.J. Harker, A.N. Morganthaler, J.R. Christensen, et al., Fascin- and alpha-actinin-bundled networks contain intrinsic structural features that drive protein sorting, Curr. Biol. 26 (20) (2016) 2697–2706.
[65] I. Van Audenhove, M. Denert, C. Boucherie, L. Pieters, M. Cornelissen, J. Gettemans, Fascin rigidity and L-plastin flexibility cooperate in cancer cell invadopodia and filopodia, J. Biol. Chem. 291 (17) (2016) 9148–9160.
[66] J.F. Krey, E.S. Krystofiak, R.A. Dumont, S. Vijayakumar, D. Choi, F. Rivero, et al., Plastin 1 widens stereocilia by transforming actin filament packing from hexagonal to liquid, J. Cell Biol. 215 (4) (2016) 467–482.
[67] T. Miyakawa, H. Shinomiya, F. Yumoto, Y. Miyauchi, H. Tanaka, T. Ojima, et al., Different Ca(2)(+)-sensitivities between the EF-hands of T- and L-plastins, Biochem. Biophys. Res. Commun. 429 (2012) 137–141.
[68] N. Daudet, M.C. Lebart, Transient expression of the t-isoform of plastins/fimbrin in the stereocilia of developing auditory hair cells, Cell Motil. Cytoskeleton 53 (2002) 326–336.
[69] E.A. Lumpkin, A.J. Hudspeth, Regulation of free Ca^{2+} concentration in hair-cell stereociia, J. Neurosci. 18 (1998) 6300–6318.
[70] J.R. Glenney Jr., A. Bretscher, K. Weber, Calcium control of the intestinal microvillus cytoskeleton: its implications for the regulation of microfilament organizations, Proc. Natl. Acad. Sci. U. S. A. 77 (1980) 6458–6462.
[71] M.S. Mooseker, T.A. Graves, K.A. Wharton, N. Falco, C.L. Howe, Regulation of microvillus structure: calcium-dependent solation and cross-linking of actin filaments in the microvilli of intestinal epithelial cells, J. Cell Biol. 87 (1980) 809–822.
[72] M. Arpin, E. Friederich, M. Algrain, F. Vernel, D. Louvard, Functional differences between L- and T-plastin isoforms, J. Cell Biol. 127 (1994) 1994–2008.
[73] J.A. Spudich, S. Watt, The regulation of rabbit skeletal muscle contraction, J. Biol. Chem. 246 (1971) 4866–4871.
[74] J. Schindelin, C.T. Rueden, M.C. Hiner, K.W. Eliceiri, The ImageJ ecosystem: an open platform for biomedical image analysis, Mol. Reprod. Dev. 82 (2015) 518–529.
[75] J. Schindelin, I. Arganda-Carreras, E. Frise, V. Kaynig, M. Longair, T. Pietzsch, et al., Fiji: an open-source platform for biological-image analysis, Nat. Methods 9 (2012) 676–682.
[76] R.R. Yu, S.K. Mahto, K. Justus, M.M. Alexander, C.J. Howard, J.J. Ottesen, Hybrid phase ligation for efficient synthesis of histone proteins, Org. Biomol. Chem. 14 (2016) 2603–2607.
[77] D.S. Kudryashov, E. Reisler, Solution properties of tetramethylrhodamine-modified G-actin, Biophys. J. 85 (2003) 2466–2475.
[78] L.A. Kelley, S. Mezulis, C.M. Yates, M.N. Wass, M.J. Sternberg, The Phyre2 web portal for protein modeling, prediction and analysis, Nat. Protoc. 10 (2015) 845–858.